Arch. Metall. Mater. **69** (2024), 1, 91-94

DOI: https://doi.org/10.24425/amm.2024.147792

HEE YEON JEON[1], MIJEONG PARK[1], SEUNGHEON HAN[1],
DONG HOON LEE[1], YOUNG-IN LEE[1*]

FACILE SYNTHESIS OF BUMPY-STRUCTURED ZnO-ZnS CORE-SHELL MICROSPHERES WITH ENHANCED PHOTOCATALYTIC PERFORMANCE

Zinc oxide is considered an outstanding photocatalyst candidate, but its low photo-corrosion resistance is a problem to be solved. In the ZnO-ZnS core-shell structure, ZnS acts as a protective layer for the ZnO core, and thus, it can enhance stability and long-term performance. The ZnO-ZnS core-shell structure is synthesized into various nanoscale morphologies with high specific surface areas to improve photocatalytic efficiency. However, they are easily agglomerated and are hard to separate from reaction media. In this study, micro-sized bumpy spheres of ZnO-ZnS core-shell structure were prepared via facile chemical transformation of as-prepared ZnO. After sulfurization of the ZnO template, it was confirmed through SEM, TEM, EDS, and XPS analysis that a uniform ZnS shell layer was formed without significant change in the initial ZnO morphology. The ZnO-ZnS core-shell microsphere has shown superior efficiency and stability in the photocatalytic degradation of Rhodamine B compared with pristine ZnO microspheres.

Keywords: ZnO; ZnS; core-shell; chemical transformation; photocatalyst

1. Introduction

Efficient purification methods are required to solve the global water pollution problem and limited water resources [1-3]. Photocatalytic water purification is considered a highly effective and efficient method for purifying water due to its advantages, including its high efficiency, energy efficiency, chemical-free process, and ease of operation [3,4]. A photocatalyst that can absorb light and convert it into chemical energy plays the most crucial role in securing the high efficiency of the purification process.

Among various materials, zinc oxide (ZnO), with a wide band gap of 3.37 eV and a large exciton binding energy of 60 meV at room temperature, has drawn considerable attention as an ultraviolet (UV)-driven photocatalyst due to its abundance, low cost, and environmental sustainability [5-9]. However, ZnO generally exhibits low photocatalytic efficiency due to rapid charge recombination and photo-corrosion dissolving as Zn^{2+} ions in an aqueous solution under UV irradiation [6,10].

One approach to overcoming the limitation is to use a ZnO-zinc sulfide (ZnS) core-shell structure, where a ZnS is coated on the surface of ZnO. The ZnS layer has higher conduction and valence band levels than ZnO and can promote the separation of photogenerated electrons and holes [5,11]. Moreover, the ZnS layer can safeguard the ZnO core, preventing photogenerated holes' accumulation and avoiding ZnO's contact with the solution [12].

The material's morphology is one of the crucial factors affecting photocatalytic efficiency. Even in the ZnO-ZnS core-shell structure, it is synthesized into various nano-sized shapes with high specific surface areas, such as nanoparticles [13], nanowires [14], and nanofibers [15], to improve photocatalytic efficiency. However, from the view of commercial applications, bumpy or hollow microspheres with a large specific surface area can be more attractive because they are easy to disperse and separate during or after photocatalytic reaction [5,16,17].

In this study, we prepared a ZnO-ZnS core-shell microsphere by chemically transforming a bumpy-structured ZnO template synthesized by an ultrasonic spray pyrolysis (USP) process. The template morphology remained unchanged during chemical transformation in a sulfuric solution. The ZnS shell was uniformly formed on the surface of ZnO, finally synthesizing a bumpy ZnO-ZnS core-shell microsphere with a size of about 1 mm. The effect of the ZnS shell layer on the photocatalytic

[1] SEOUL NATIONAL UNIVERSITY OF SCIENCE AND TECHNOLOGY, DEPARTMENT OF MATERIALS SCIENCE AND ENGINEERING, SEOUL 01811, REPUBLIC OF KOREA

* Corresponding author: youngin@seoultech.ac.kr

efficiency and photo-corrosion resistance was evaluated by monitoring the degradation of rhodamine-B (Rh-B) under irradiation with a xenon lamp, and the core-shell microspheres showed better efficiency and stability than pristine ZnO.

2. Experimental

The bumpy-structured ZnO template was synthesized by the USP process described in previously reported literature [18]. Briefly, the aqueous solution with 100 mM of $Zn(CH_3COO)_2 \cdot 2H_2O$ (99.9%, Sigma-Aldrich) was ultrasonically sprayed into droplets, which were then carried into a tube furnace at 500°C to produce ZnO powders through solvent evaporation and precursor decomposition. A filter paper collected the synthesized powder. Chemical transformation of the ZnO template to ZnO-ZnS core-shell microsphere was conducted by placing the ZnO powder into an aqueous sulfur precursor solution with 100 mM thiourea (CH_4N_2S, >99.0%, Sigma-Aldrich) for 12 h at a temperature of 60°C. The transformed product was washed with DI water and dried at 30°C for 24 h.

The morphology, crystal structures, and microstructure of the transformed product were characterized by X-ray diffraction (XRD, X'Pert3 Powder, PANalytical, Netherlands), field emission scanning electron microscopy (FE-SEM, S-4800, Hitachi, Japan), and high-resolution transmission electron microscopy (HR-TEM, JEM-2100F, JEOL, Japan). The elemental composition of the sample was analyzed using X-ray photoelectron spectroscopy (XPS, K-Alpha+, Thermo Fisher Scientific, United States) and energy-dispersive spectroscopy (EDS, JED-2300, JEOL, Japan). The photocatalytic activity of the pristine ZnO and chemically transformed ZnO-ZnS core-shell powders was evaluated by measuring the degradation rate of Rh-B. The photocatalytic experiments were performed using 100 mL of a 0.5×10^{-5} M aqueous Rh-B solution with 0.10 g of the powders and about one sun irradiation generated by a solar simulator with a 300 W xenon lamp. After the photocatalytic reaction, the residual concentration of Rh-B was determined by a UV-vis spectrometer (UV-vis DRS, UV-2600, SHIMADZU, Japan) based on the Beer-Lamber law [18]. Five test cycles for photocatalytic activity were carried out using the same process to determine the stability against photo-corrosion.

3. Results and discussion

Fig. 1(a) and (b) show representative FE-SEM images of the synthesized templates indicating that the powder consisted of polydispersed microspheres ranging from several hundred nanometers to 2 μm in diameter and exhibited dimples and wrinkles [18]. The FE-SEM images in Fig. 1(c) and (d) show the chemically transformed products by the aqueous thiourea solution from the initial templates. The images show that their size range and morphology with dimples and wrinkles were maintained after the sulfurization process. The crystal structures of the template and chemically transformed products were characterized by XRD, as shown in Fig 1(e). The templates have diffraction peaks indexed to the hexagonal wurtzite ZnO structure (JCPDS card No. 05-0664). After the sulfurization of the template, the product shows mixed diffraction peaks of the hexagonal wurtzite ZnO and ZnS (JCPDS card No. 01-0792).

Fig. 2 shows the TEM and EDS analysis results of the ZnO-ZnS sample in which ZnO was partially converted to ZnS through the chemical transformation in the aqueous sulfuric solution. Through this analysis, we can more clearly confirm the shape of the particles. The sample had a structure with a hollow interior and a wrinkled and pitted surface. As previously explained, the size and shape of the ZnO-ZnS powder increase the amount of surface area available, reduce agglomeration, and make it easier to separate the product after the photocatalytic reaction. In the EDS mapping results, sulfur was clearly observed. Moreover, the detecting area for sulfur was more expansive than the oxygen-detecting area, confirming that ZnO and ZnS form a core and a shell, respectively. The change of chemical bonding

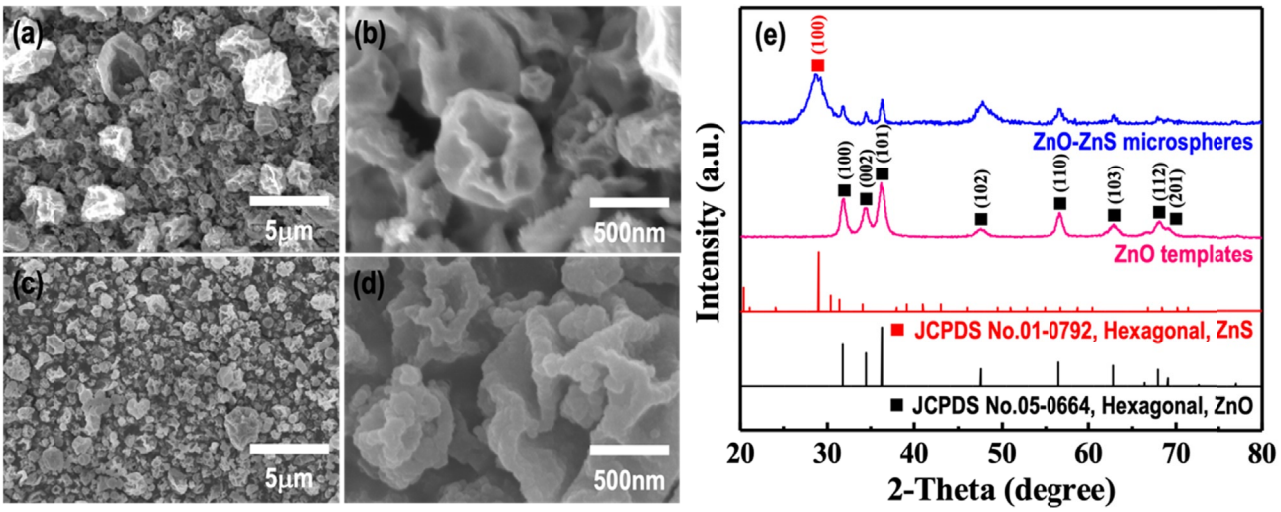

Fig. 1. FE-SEM images of (a, b) bumpy-structured ZnO templates synthesized by an ultrasonic spray pyrolysis and (c, d) bumpy ZnO-ZnS microspheres chemically transformed from the ZnO templates in aqueous thiourea solution. (e) is the X-ray diffraction patterns of the samples

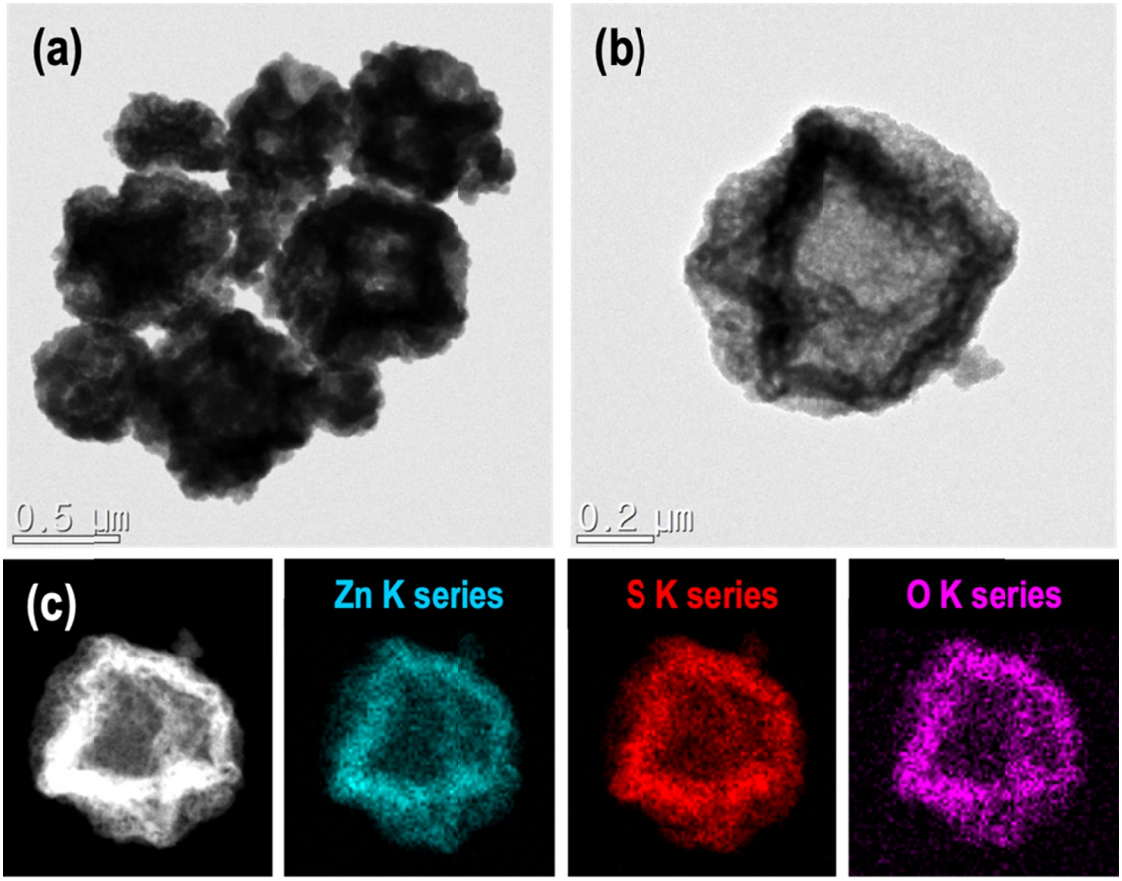

Fig. 2. (a, b) TEM images and (c) STEM images and EDS elemental mapping results of the ZnO-ZnS microspheres

state on the chemical transformation from ZnO to ZnO-ZnS was investigated by XPS analysis. As shown in Fig. 3(c), the peak for S 2p was observed in ZnO-ZnS core-shell powder. Thus, the conversion from ZnO to ZnS was confirmed. In addition, there is evidence for the transformation, such as the shift of Zn 2P and O 1s to the higher binding energy, as shown in Fig. 3(a) and (b) [5,15].

The photocatalytic removal rate of Rh-B over the ZnO and ZnO-ZnS core-shell powders was confirmed by a pseudo-first-order kinetics reaction with a simplified Langmuir-Hinshelwood model when Co is very small [19]. As shown in Fig. 4(a) and (b), the core-shell powder shows a faster removal rate than the pristine ZnO powder. The apparent rate constant k of the ZnO-ZnS core-shell powder is 0.102 min^{-1}, 2.7 times that of the ZnO powder (k = 0.038 min^{-1}). This result shows that a typical type-II heterojunction that promotes the separation of electrons and holes generated by the photon was well built in the ZnO-ZnS core-shell microsphere. Thus, enhanced photocatalytic activity is observed.

The degradation test of Rh-B was repeated for five cycles to evaluate the photo-corrosion stability during the photocatalytic degradation of Rh-B. Fig. 4(c) and (d) show the reuse stability of the bumpy-structured ZnO and ZnO-ZnS core-shell microspheres through the degradation graphs by plotting the C/C_0 graph according to the irradiation time about each cycle, respectively. In the case of the pristine ZnO sample, the degradation efficiency decreased as the cycle repeated. However, ZnO-ZnS core-shell microspheres show no significant decrease in photodegradation activity after five consecutive cycles. The degradation efficiency after five cycles is still near 100%, indicating that

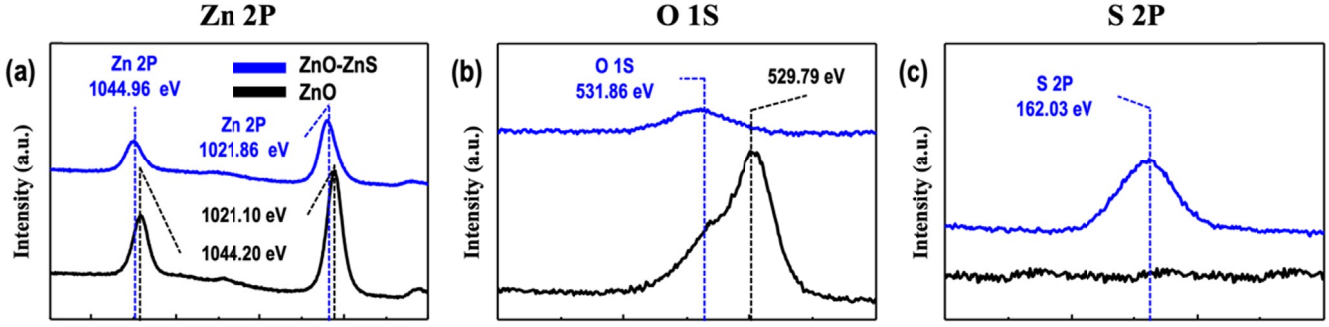

Fig. 3. XPS spectra of the as-prepared ZnO templates and ZnO-ZnS core-shell microspheres: (a) Zn 2P, (b) O 1S and (c) S 2P

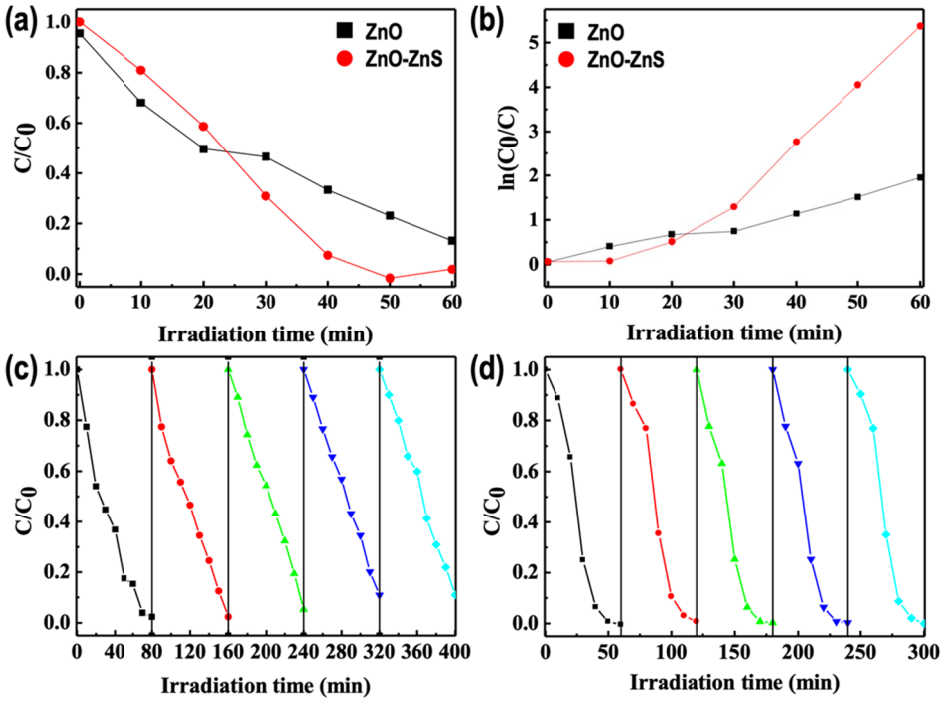

Fig. 4. (a) Kinetics, (b) first-order linear transforms $\ln(C/C_0) = kt$ of Rh-B and (c, d) cycling test results by (c) pristine ZnO and (d) chemically transformed ZnO-ZnS core-shell microspheres

the ZnO-ZnS core-shell microsphere shows excellent stability and recyclability and that the ZnS shell plays a protective layer for the ZnO core.

4. Conclusion

In summary, we have successfully synthesized the ZnO-ZnS core-shell microsphere via the facile chemical transformation of ZnO templates prepared by the USP process. It had a structure with a hollow interior and a wrinkled and pitted surface for maximizing the specific surface area, suppressing aggregation, and facilitating separation after the photocatalytic reaction. The EDS mapping and XPS analysis confirmed the core-shell structure with the uniform ZnS shell layer. The bumpy-structured ZnO-ZnS core-shell microsphere quickly degraded the Rh-B dye molecules, which shows 2.7 times the photocatalytic performance of the pristine ZnO microsphere. Furthermore, the core-shell structure also shows good reusability and the degradation efficiency is maintained near 100% after five cycles. The results demonstrated the potential application of the bumpy-structured ZnO-ZnS core-shell microsphere in wastewater remediation. This proposed methodology thus demonstrates great potential for synthesizing shape-controlled core-shell microspheres with excellent photocatalytic activity.

Acknowledgments

This study was supported by the Research Program funded by the SeoulTech(Seoul National University of Science and Technology).

REFERENCES

[1] U.I. Gaya, A.H. Abdullah, J. Photochem. Photobiol. C **9**, 1 (2008).
[2] P.R. Gogate, A.B. Pandit, Adv. Environ. Res. **8**, 501 (2004).
[3] J. Low, J. Yu, M. Jaroniec, S. Wageh, A.A. Al-Ghamdi, Adv. Mater. **29**, 1601694 (2017).
[4] A. Kudo, Y. Miseki. Chem. Soc. Rev. **38**, 253 (2009).
[5] L. Yu, W. Chen, D. Li, J. Wang, Y. Shao, M. He, P. Wang, X. Zheng, Appl. Catal. B: Environ. **164**, 453 (2015).
[6] C. Hariharan, Appl. Catal. A: Gen. **304**, 55 (2006).
[7] M.D. Driessen, T.M. Miller, V.H. Grassian J. Mol. Catal. A: Chem. **131**, 149 (1998).
[8] Y. Jo, C.Y. Woo, S.K. Hong, H.W. Lee, J. Powder Mater. **27**, 305 (2020).
[9] D.C. Look, Mater. Sci. Eng. B-Adv. Funct. Solid-State Mater. **80**, 383 (2001).
[10] L. Wang, X. Hou, F. Li, G. He, L. Li, Mater. Lett. **161**, 368 (2015).
[11] J. Lahiri, M. Batzill, J. Phys. Chem. C **112**, 4304, (2008).
[12] Z. Guo, W. Huo, T. Cao, X. Liu, S. Ren, J. Yang, H. Ding, K. Chen, F. Dong, Y. Zhang, J. Colloid Interface Sci. **588**, 826 (2021).
[13] A. Sadollahkhani, I. Kazeminezhad, J. Lu, O. Nur, L. Hultman, M. Willander, RSC Adv. **4**, 36940 (2014).
[14] X. Gao, J. Wang, J. Yu, H. Xu, Cryst. Eng. Comm. **17**, 6328 (2015).
[15] K.S. Ranjith, A. Senthamizhan, B. Balusamya, T. Uyar, Catal. Sci. Technol. **7**, 1167 (2017).
[16] J. Yu, W. Liu, H. Yu, Cryst. Growth Des. **8**, 930 (2008).
[17] X. Yang, H. Liu, T. Li, B. Huang, W. Hu, Z. Jiang, J. Chen, Q. Niu, Int. J. Hydrog. Energy **45**, 26967 (2020).
[18] Y. Choi, Y.-I. Lee, J. Korean Ceram. Soc. **55**, 261 (2018).
[19] J.-H. Yoo, M. Ji, J.H. Kim, C.-H. Ryu, Y.-I. Lee, J. Photochem. Photobiol. A **401**, 112782 (2020).